High Current C-11 Gas Target Design and Optimization Using Multi-Physics Coupling

J. L. Peeples[1, a)], M. Magerl[2], E. M. O'Brien[3], J. M. Doster[3], I. A. Bolotnov[3], B. W. Wieland[1] and M. H. Stokely[1, b)]

[1]*BTI Targetry LLC, 1939 Evans Road Cary, NC 27513 USA*
[2]*IBA Molecular North America, 21000 Atlantic Boulevard Suite 730 Dulles, VA 20166*
[3]*North Carolina State University, Raleigh, NC 27695*

[a)]Corresponding author: peeples@btitargetry.com
[b)]stokely@btitargetry.com

Abstract. A high current conical C-11 gas target with a well characterized production yield was designed and optimized using multi-physics coupling simulations. Two target prototypes were deployed on an IBA 18/9 cyclotron, and the experimental results were used to benchmark the predictive simulations.

INTRODUCTION

The primary goal of this project was to implement a predictive simulation method to develop a high current C-11 target system for the IBA 18/9 cyclotron. Two prototype geometries were designed and used to benchmark the technique. Target design constraints included a gas volume less than 80 cm^3, based on existing commercial designs, and an operating pressure less than 50 bar (725 psi), to provide a factor of two safety margin with respect to cold burst pressure of the window foil. The target operating pressure constraint corresponds to a maximum target pre-pressure of roughly 14 bar (200 psi). The main objective was to maximize saturation yield without exceeding the volume and pressure constraints.

The predictive simulations were used to generate three-dimensional distributions of reaction rate density. The dimensions of the conical gas chamber were optimized with respect to the yield distribution in such a way that regions with significant contributions to yield were included, while regions with small yield contributions were excluded to maintain a reasonable system volume. Minimally, any increase in gas volume has a corresponding increase in recovery time, such that additional volume in a low yield density region could easily result in a net decrease in recovered activity due to decay. Additional volume can also result in reduced specific activity.

Due to the 3.22 MeV threshold energy for the $^{14}N(p,\alpha)^{11}C$ reaction, the ideal target geometry is not range-thick to protons. Less than 2% of the yield is produced by protons between 0-6 MeV, although they account for one third of the heat input to the target. To maintain a reasonable target volume, protons of reduced energy (that no longer have significant cross-section) stream out of the radial and back walls of the target chamber. Effective target depth can be increased by raising the operating pressure of the nitrogen gas, thus increasing the target mass and stopping power. However, maximum operating pressure is limited by the failure point of the target window.

MATERIALS AND METHODS

Two conical target designs were simulated, and four total configurations were fabricated and experimentally tested. For each design a smooth wall and rough wall target was constructed. For the rough wall cases, the Roughness Average (Ra) was increased from roughly 3 μm (for the smooth wall targets) to more than 100 μm. Both conical designs had a chamber depth of 25 cm and a diameter at the window of 1.2 cm. Prototype 1 had a diameter at the back wall of 2.24 cm, while the taper angle of Prototype 2 was increased to result in a diameter at the back wall of 2.72 cm. The chamber walls of each aluminum target body were cooled using four 6.1 mm water channels, and the principal (38 μm Havar) and vacuum (25 μm

Havar) windows were cooled using conventional helium recirculation through directed jets. Preliminary calculations showed that neither single foil nor gridded single foil are appropriate alternatives to helium cooling for both high current and energies above 11-12 MeV. Initially, Prototype 1 was experimentally tested and used to benchmark predictive multi-physics simulations of target density and saturation yield. Simulation results were then used to select an appropriate taper angle for Prototype 2. Experimental testing of Prototype 1 included nitrogen loading pressures between 10 and 16 bar (150-230 psi) and beam currents up to 110 μA.

The multi-physics modeling technique includes explicit coupling of radiation transport and associated stopping power/heat deposition (MCNPX) to computational fluid dynamics (CFD) modeling of the gas density profile and resulting convective currents (ANSYS Fluent), [1,2]. An initial input deck can be supplied to MCNPX assuming an average nitrogen density for the gas chamber. An MCNPX mesh tally of the nitrogen gas is used to generate a 3D heat generation profile of roughly 150,000 points that is supplied to ANSYS Fluent. ANSYS Fluent uses temperature-dependent values for nitrogen density, specific heat, thermal conductivity, and viscosity at specified average pressure. The material properties were determined using the NIST Chemistry Webbook [3] and supplied in tabular form. The CFD calculation models the convective currents in the gas target [4,5] and generates the three-dimensional nitrogen density profile resulting from the specified heat profile, pressure and temperature-dependent material properties, and cooling boundary conditions. Average target pressure can be adjusted to achieve the desired total system mass of nitrogen. The nitrogen density profile is extracted from ANSYS Fluent and used to generate a non-uniform density profile for MCNPX. The nitrogen volume is divided in MCNPX into roughly 50,000 cells, and each cell assigned the corresponding density from ANSYS Fluent. Information is passed between the radiation transport and CFD codes in an iterative fashion until a converged density profile is achieved, as illustrated in Fig. 1.

Each iteration approaches the final solution in an oscillatory manner due to the tight coupling between target density profile and stopping power/beam heating. For this range-thin system, energy deposition in the nitrogen region is not a fixed fraction of the beam current. If the heat input is overestimated for the nitrogen region in the CFD simulation, the density profile will be under-predicted along the central axis. When the density is underestimated along the central axis in the radiation transport simulation, the beam will reach the back of the target at a higher energy, and the heat input in the nitrogen region will be under-predicted. Despite the oscillatory nature, the simulation is stable and convergent. The convergence rate can be increased by using successive under-relaxation (SUR) of the density profile supplied to MCNPX, while maintaining an equivalent converged solution. Use of SUR was shown to decrease total solution convergence time by roughly a factor of two.

This multi-physics method was originally applied to a liquid F-18 target at very low beam current and presented at the WTTC 15 workshop [6]. The liquid target simulation was limited to low beam current because modeling of the phase change (boiling water) is too computationally expensive for available resources at this time. The method is better suited to modeling a gas target, because there is no phase change. It has also been successfully applied to a $^{20}Ne(d,\alpha)^{18}F$ target [7].

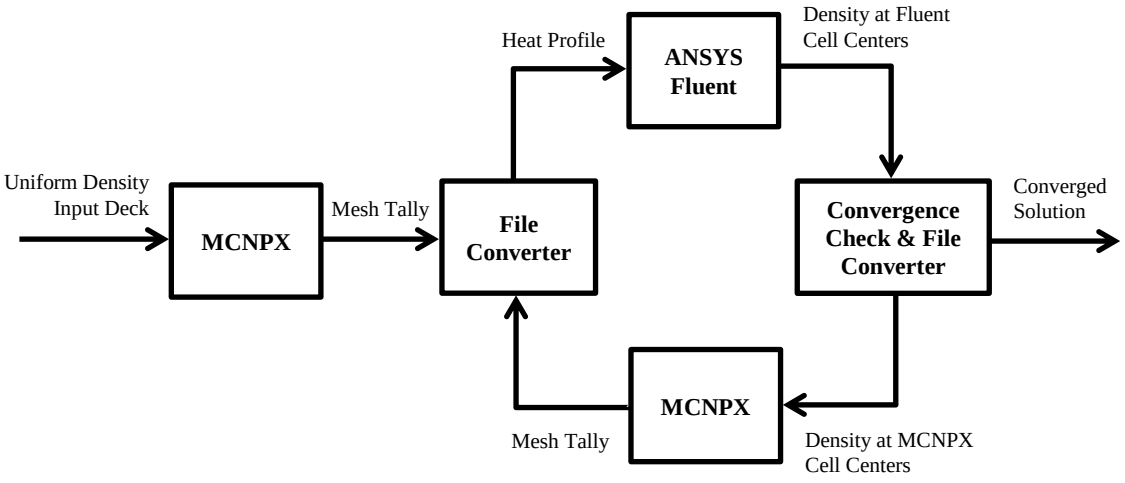

FIGURE 1. Flow chart of multi-physics method

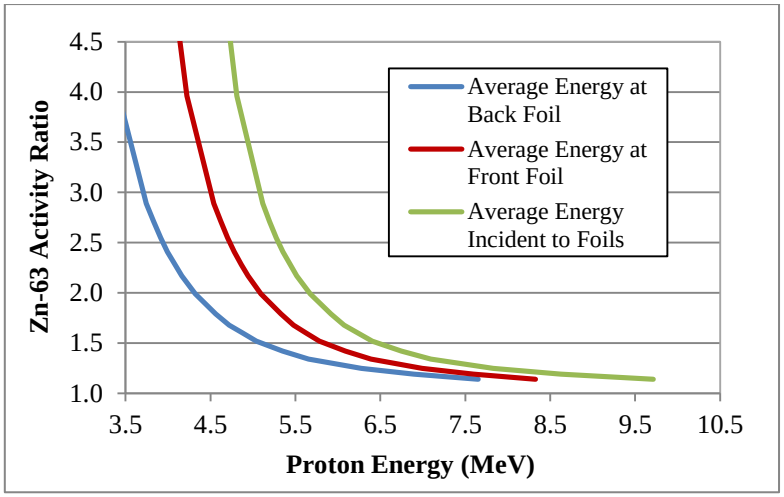

FIGURE 2. Activity ratio vs. average proton energy.

The converged solution is used to generate a three-dimensional distribution of reaction rate in the target. This both accurately predicts the total product yield and provides insight for geometry optimization. Total solution convergence time is roughly 16 hours, with a 3.7 Ghz Intel i7 eight core enhanced performance processor. Due to computational expense, only smooth wall target designs were simulated.

An experimental benchmark was performed using smooth wall Prototype 1 for four experimental cases. Two simulation constraints were selected to benchmark C-11 saturation yield for the model and experiment, nitrogen mass and transmitted energy spectrum. By adjusting the material properties table in ANSYS Fluent, it is possible to align the simulation to one of the two constraints, but not both. Nitrogen mass is a function of known initial temperature and pre-pressure. To measure the transmitted energy spectrum, two copper foils of 25 μm thickness were stacked in the back of the target chamber. The ratio of Zn-63 activity produced in each copper foil can be used to estimate the average energy of protons which strike the back wall of the target [8]. The two copper foils were included in the MCNPX simulation, and the foil activation ratio was used as an additional benchmark constraint. The transmitted energy range that produces a useful ratio, roughly 4.5 to 6.5 MeV, corresponds well with the reaction threshold.

For a constant gas pressure, material properties are strictly temperature-dependent. CFD system pressure was adjusted for each experimental benchmark case to achieve the same total mass or the same foil activation ratio (with estimated average proton energy striking the back wall within 200 keV of experimental value) as the experimental condition for the specified beam current. Average incident proton energy on the first copper foil and average energy within each foil for the resulting spectrum was predicted using MCNPX and is shown in Fig. 2.

RESULTS AND CONCLUSIONS

Internal gas pressure (P_{beam}) as a function of beam current was measured for Prototype 1 for three initial pressure conditions, as shown in Fig. 3(a), and for one initial pressure condition for Prototype 2, as shown in Fig. 3(b). Saturation yield values were measured using a combination of soda lime, molecular sieve, and gas sequestration traps. Approximately 90% of the C-11 activity was delivered in the form of carbon dioxide. Saturation yield measurements are compared to simulation results in Fig. 4. The simulation predicts total saturation yield of C-11, so the plotted simulation values have been reduced to 90% to account for the recovered fraction as $^{11}CO_2$ and provide a direct comparison to the experimental data. There are two simulation results for each benchmark condition, corresponding to the transmitted energy spectrum and nitrogen mass constraints. For all cases, the energy spectrum constraint predicted a 5% lower saturation yield than the mass constraint.

A benchmark between the four experimental cases and multi-physics simulation results is shown in Table 1. For each case, two simulation results are generated. For case A, the simulation density is within 1.5% of the experimental density, and for case B, the predicted foil activation ratio corresponds to an estimated average energy incident on the first copper foil within 200 keV of the experimental value. The simulation predicts total saturation yield of C-11, so the simulation values have been reduced to 90% to account for the recovered fraction as $^{11}CO_2$ and provide a direct comparison to the experimental data. All simulations following the initial benchmark employ the nitrogen mass constraint, which is simpler to implement both experimentally and computationally.

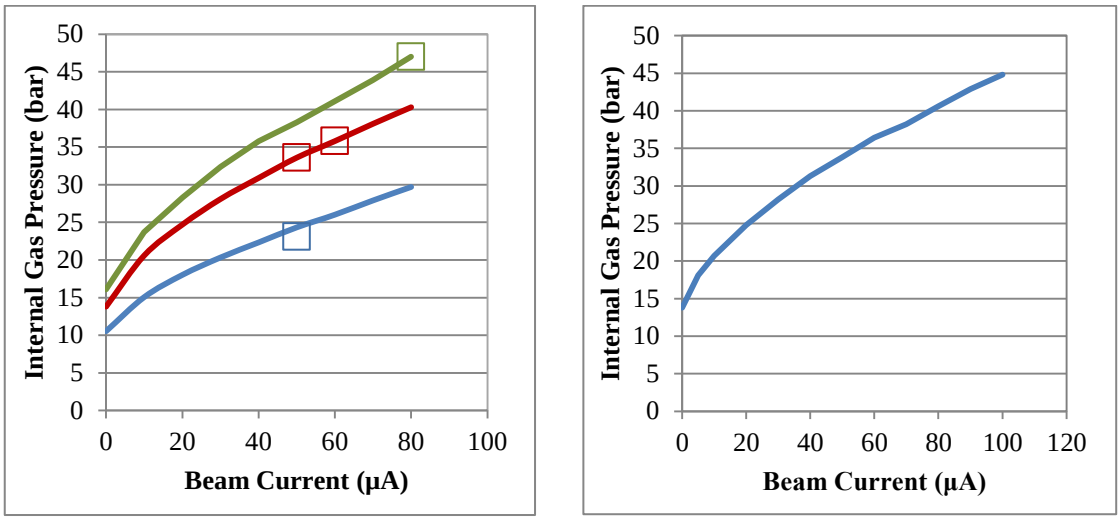

FIGURE 3. Internal gas pressure vs. beam current for (a) Prototype 1 with benchmark conditions marked as boxes and (b) Prototype 2

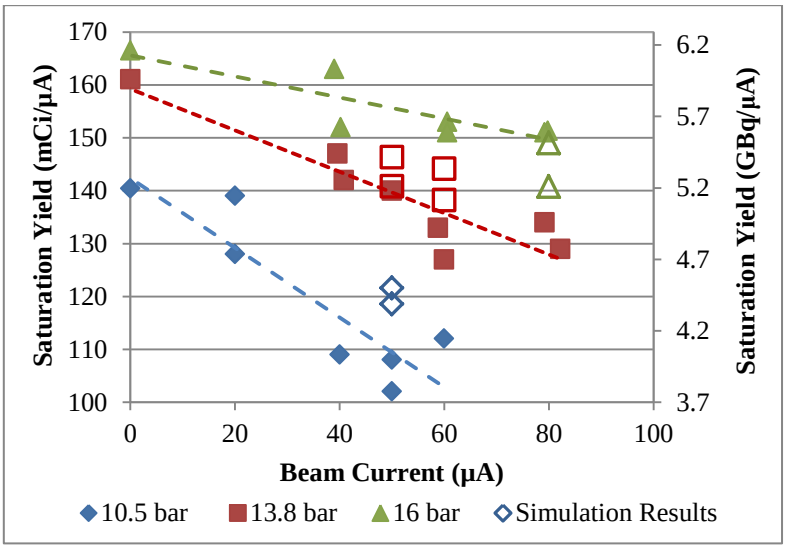

FIGURE 4. $^{11}CO_2$ saturation yield vs. beam current with open symbols for simulation results

TABLE 1. Benchmark of multiphysics method to experiment results

Case	I	P_0		Mass	ρ_{AVG}	P_{beam}		Ratio	$^{11}CO_2$ Saturation Yield	
	(μA)	(bar)	(psi)	(g)	(kg/m^3)	(bar)	(psi)	(-)	(GBq/μA)	(mCi/μA)
Experiment 1	**80**	**16.0**	**232**	**1.10**	**18.4**	**47.0**	**682**	**2.10**	**5.54**	**149.7**
Model - A1	80	-	-	1.11	18.5	-	-	8600	5.51	149.0
Model - B1	80	-	-	0.931	15.5	-	-	2.06	5.21	140.8
Experiment 2	**60**	**13.8**	**200**	**0.952**	**15.9**	**35.8**	**519**	**1.63**	**5.02**	**135.7**
Model - A2	60	-	-	0.940	15.7	-	-	3.27	5.34	144.2
Model - B2	60	-	-	0.866	14.4	-	-	1.61	5.11	138.2
Experiment 3	**50**	**13.8**	**200**	**0.952**	**15.9**	**33.6**	**487**	**1.79**	**5.17**	**139.7**
Model - A3	50	-	-	0.951	15.8	-	-	5.95	5.41	146.3
Model - B3	50	-	-	0.872	14.5	-	-	1.82	5.21	140.9
Experiment 4	**50**	**10.5**	**152**	**0.726**	**12.1**	**24.3**	**353**	**1.15**	**4.05**	**109.4**
Model - A4	50	-	-	0.730	12.2	-	-	1.17	4.50	121.6
Model - B4	50	-	-	0.709	11.8	-	-	1.15	4.38	118.5

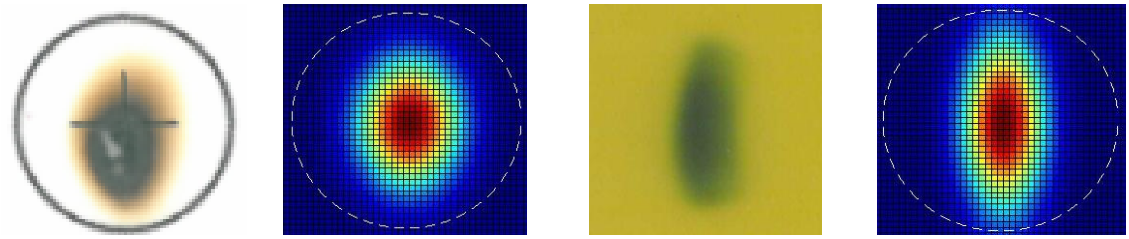

(a) (b) (c) (d)

FIGURE 5. (a) Paper burn of beam profile with (b) simulated beam profile and (c) GAF ChromicFilm radiograph of beam profile with (d) more peaked simulated beam profile

Beam shape was measured experimentally using a paper burn at the front window plane, as shown in Fig. 5(a), and the MCNPX input deck source specification was adjusted to match the experimental profile. The MCNPX beam profile, shown in Fig. 5(b), had $FWHM_X$ = 0.564686 cm and $FWHM_Y$ = 0.423632 cm, corresponding to a measured 93% transmission in 10 mm diameter and the approximate shape of the experimental paper burns. This beam profile was used for all simulation results presented in this work. More recent experiments have shown more vertical skew with a 20% increase in beam peaking, as shown in Fig. 5(c). Select cases were repeated using the more peaked beam profile, shown in Fig. 5(d), resulting in predicted saturation yields within 1% of the original values. This indicates that the simulation is fairly insensitive to beam shape with respect to saturation yield predictions.

Nitrogen temperature along the vertical and horizontal mid-planes is shown in Fig. 6 for case A1 at 80 μA and 16 bar pre-pressure. Nitrogen density is strictly a function of temperature with lower density in the regions of higher temperature. Higher temperature in the top of the target is a result of convective currents in the nitrogen gas (clockwise in Fig. 6).

Figure 7 shows the linear yield density, or saturation yield per unit length, which illustrates the relative contribution to yield of each nitrogen region as a function of depth. This allows for optimization of the chamber dimensions, including selection of appropriate target depth. Maximum linear density occurs around 11-12 cm. High reaction rate near the radial wall at this position motivated the increased taper angle for Prototype 2. The yield density distribution, shown in Fig. 8, offers similar information and insight, but with considerably more detail, as the spatial dependence is three-dimensional.

Figure 7 and Fig. 8 illustrate that this target design is not optimized for case A1, because it includes unnecessary volume in the back. This suggests that the target could be operated at higher beam current for the same initial pressure, at the same beam current with a reduced initial pressure (to provide additional safety margin for the window), or that the target depth (and therefore volume) could be reduced for the same beam current and initial pressure to better optimize production yield.

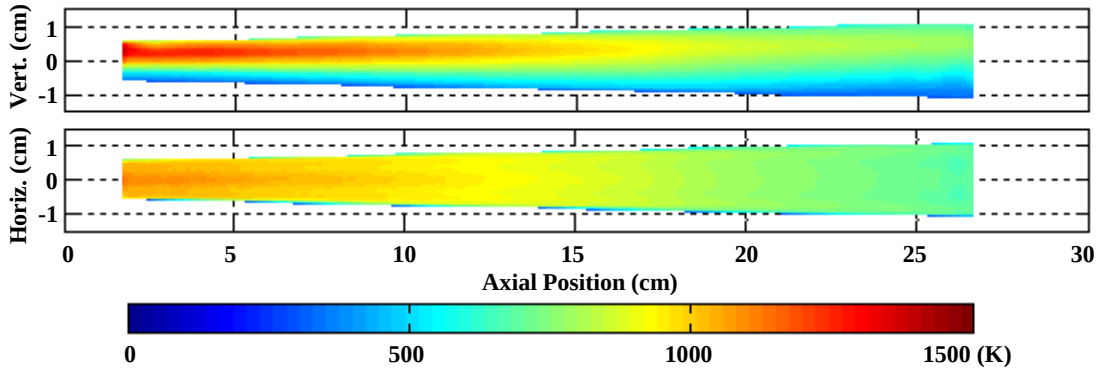

FIGURE 6. Nitrogen temperature along vertical and horizontal mid-planes for case A1 (80 μA and 16 bar)

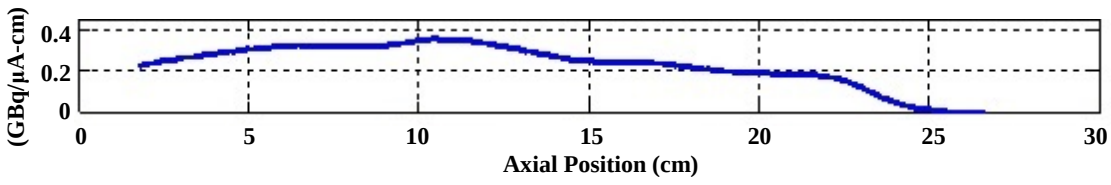

FIGURE 7. Linear yield density distribution for case A1 (80 μA and 16 bar)

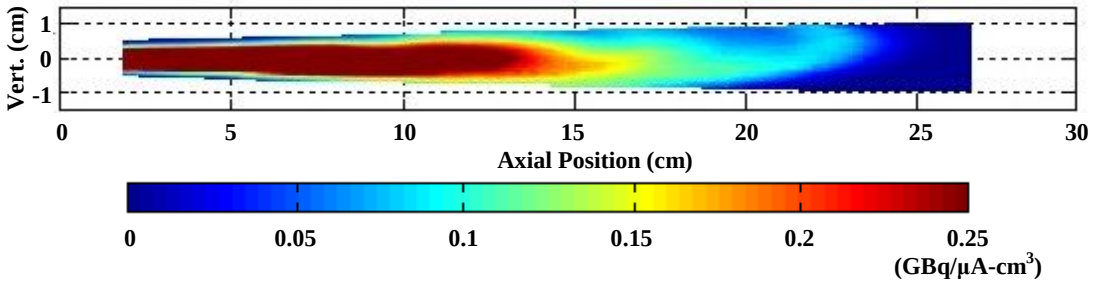

FIGURE 8. Yield density distribution along vertical mid-plane for case A1 (80 μA and 16 bar)

The yield density, shown in Fig. 8, indicates the region of the reaction threshold, with a shape consistent with published visible light images of gas targets [9,10].

Experimental saturation yield for the two prototype targets is compared to the simulation predictions in Fig. 9. Only the smooth wall prototypes were simulated due to the computational expense associated with modeling the wall roughness. For both prototypes, the simulation over-predicts $^{11}CO_2$ saturation yield by approximately 10%. Prototype 2 produces a higher saturation yield than Prototype 1, as predicted by the model, and as seen in Fig. 10. This can be primarily attributed to less proton escape through the radial walls.

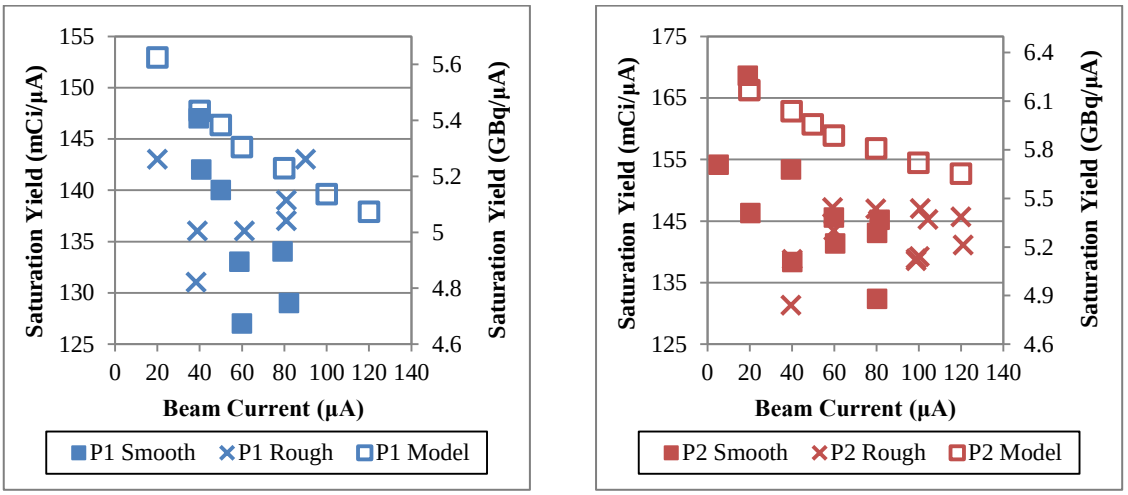

FIGURE 9. $^{11}CO_2$ saturation yield for (a) Prototype 1 and (b) Prototype 2

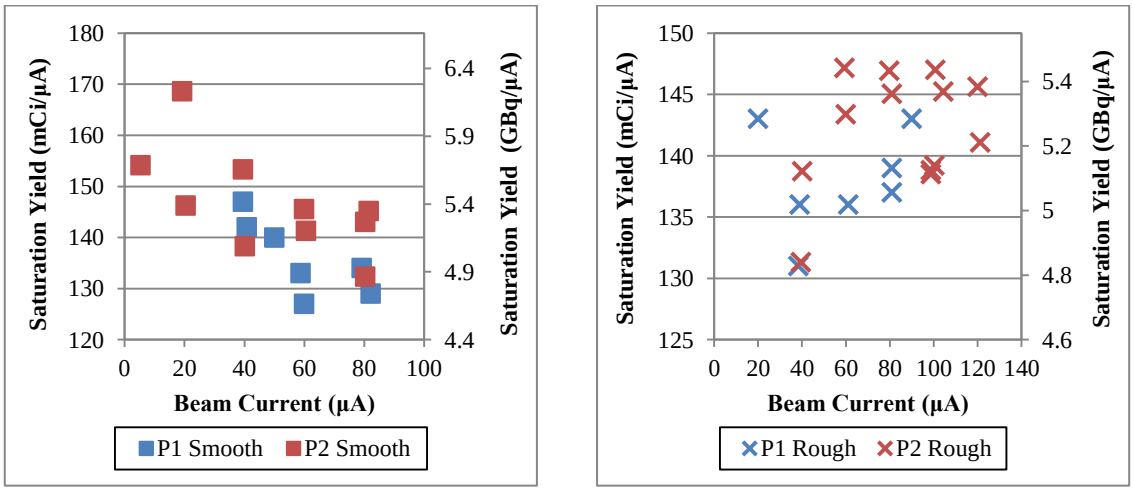

FIGURE 10. Experimental $^{11}CO_2$ saturation yield for (a) smooth wall prototypes and (b) rough wall prototypes

The prototype targets were capable of producing significant amounts of $^{11}CO_2$. The largest single production run produced 410 GBq (11 Ci) for a 30 minute irradiation at 120 μA using the rough wall Prototype 2.

The described multi-physics modeling technique has proven to be a valuable tool for gas target design and optimization. For this application, the ideal target geometry is yield-thick, but range-thin. The simulation package was successfully benchmarked using two prototype targets. Additional benchmark experiments and model refinements are planned to improve the predictive capabilities.

ACKNOWLEDGEMENTS

The authors would like to thank Gerald T. Bida for his contributions, including best practices and methodology regarding gas targets generally and C-11 targets specifically.

REFERENCES

1. D.B. Pelowitz, Ed., "MCNPX User's Manual Version 2.7.0" LA-CP-11-00438, 2011.
2. ANSYS Fluent, Release 16.1.
3. P.J. Linstrom and W.G. Mallard, Eds., *NIST Chemistry WebBook*, NIST Standard Reference Database Number **69**, Natl. Inst. of Standards and Tech., http://webbook.nist.gov, (retrieved April 2016).
4. D.J. Schlyer, S.-J. Heselius and A.P. Wolf, "Temperature Distribution in a Gas Target during Irradiation," in WTTC 2 Proceedings, (Heidelberg, West Germany, 1987), pp. 12-14.
5. S.-J. Heselius, P. Malmborg, O. Solin and B. Långström, Appl. Radiat. Isot. **38**(1), 49-57 (1987).
6. T. Faugl, M. Stokely, B. Wieland, I. Bolotnov, J. Doster, J. Peeples and M. Poorman, "Modeling a Water Target with Proton Range and Target Density Coupling," in WTTC 15 Proceedings, (Prague, Czech Republic, 2014).
7. E. O'Brien, M.H. Stokely, J.M. Doster and I.A. Bolotnov, "Multi-Physics Coupling for Optimization of Cyclotron Targetry," in ANS Conference Proceedings, (Washington D.C., US, 2015).
8. K. Gagnon, M. Jensen, H. Thisgaard and T.J. Ruth, Appl. Radiat. Isot. **69**(1), 247-53 (2010).
9. F. Tárkányi, S. Takács, S.-J. Heselius, O. Solin and J. Bergman, Nucl. Instr. Meth. Phys. Res. A **397**, 119-124 (1997).
10. S.-J. Heselius, P. Lindblom and O. Solin, Int. J. Appl. Radiat. Isot. **33**, 653-659 (1982).